

1 **Comparison of Proxy and Multi-Model Ensemble Means on Volcanic Aerosols'**
2 **Hydrological Effects in Asian Monsoon and Westerlies-dominated Subregions**
3 **Z. Zhuo¹, C.C. Gao², I. Kirchner¹ and U. Cubasch¹**

4 ¹Institute of meteorology, Freie Universität Berlin, Berlin, Germany.

5 ²Department of Environmental Science, Zhejiang University, Hangzhou, China.

6
7 Corresponding author: Zhihong Zhuo (zhihong.zhuo@met.fu-berlin.de)

8
9 **Key Points:**

- 10 • Proxy and multi-model ensemble means agree/disagree on post-volcanic hydro-responses
11 over the Asian monsoon/westerlies-dominated subregions
- 12 • Better agreement of spatial hydrological patterns is suggested in one year after the
13 eruption and in subregions with more tree ring data
- 14 • Multi model ensemble means can reproduce the hydrological response to volcanic
15 perturbations in southern Asian monsoon region

16 Abstract

17 Proxy-model comparisons show large discrepancies on volcanic aerosols' hydrological effects in
18 the Asian monsoon region (AMR). This was mostly imputed to uncertainties of the single model
19 used in previous studies. Here, we compared two groups of CMIP5 multi-model ensemble mean
20 (MMEM) with the tree-ring-based reconstruction Monsoon Asia Drought Atlas (MADA PDSI),
21 to examine their reliability on reflecting hydrological effects of the volcanic eruptions in 1300-
22 1850 CE. Time series plots indicate that MADA PDSI and MMEMs agree on the significant
23 drying effects of volcanic perturbation over the monsoon-dominated subregion, while
24 mismatches exist over the westerlies-dominated subregion. Comparisons on spatial patterns
25 suggest that MADA PDSI and MMEMs agree better in one year after the volcanic eruption than
26 in the eruption year, and in subregions with more available tree ring chronologies. MADA PDSI
27 and CMIP5 MMEMs agree on the drying effect of volcanic eruptions in western-East Asia,
28 South Asian summer monsoon and northern East Asian summer monsoon (EASM). Model
29 results suggest significant wetting effect in southern EASM and western-South Asia, which
30 agrees with the observed hydrological responses to 1991 Mount Pinatubo eruption. Analysis on
31 LME model simulations show similar hydrological responses. These results suggest that CMIP5
32 MMEM is able to reproduce volcanic eruptions' hydrological effects in southern AMR.

33 1 Introduction

34 Large explosive volcanic eruptions inject a large amount of sulfur into the stratosphere.
35 After being converted to sulfate aerosols, they significantly cool the Earth's surface and warm
36 the stratosphere by reflecting incoming solar radiation and absorbing both solar and longwave
37 radiation (Robock 2000, 2015). Both observation and model results show that the direct surface
38 cooling effects in summer (Kirchner et al., 1999) lead to significant summer precipitation
39 reduction, especially in African and Asian monsoon regions (Trenberth & Dai, 2007; Iles et al.,
40 2013; Iles & Hegerl, 2014; Zambri & Robock, 2016).

41 The Asian monsoon region (AMR, 8.75°S–56.25°N, 61.25°E–143.75°E, Cook et al.,
42 2010) covers the most populated countries like China and India. The AMR has an uneven
43 precipitation distribution due to different dominant winds, with much larger precipitation in the
44 monsoon-dominated subregion (MDSR, southeast) than in the westerlies-dominated subregion
45 (WDSR, northwest). Understanding the hydrological variation of volcanic perturbation in the
46 AMR, is both biophysically and socioeconomically important (Dando, 2005). However, only
47 limited studies aimed at this region, like Anchukaitis et al. (2010), Zhang et al. (2012), Man et al.
48 (2014), Zhuo et al. (2014) and Stevenson et al. (2016, 2017), which investigated hydrological
49 effects of historical volcanic eruptions in the past centuries. None of these studies took different
50 dominated subregions into consideration in analysis. Their results show discrepancy even
51 inversed spatial distribution of the hydrological effects between proxy reconstruction and single
52 model simulation. The discrepancy was mostly imputed to model uncertainties due to a biased
53 trust in proxy data. This can limit studies based on model simulations to understand potential
54 mechanisms of volcanic aerosols' hydrological effects in this region. Proxy reconstructions also
55 have uncertainty (PAGES 2k–PMIP3 group, 2015). PAGES Hydro2k Consortium (2017)
56 suggests an equal view toward the uncertainties and limitations of proxy and models when
57 comparing them with each other.

58 Recent studies report that an ensemble approach leads to a better estimation of climate
59 change as it averages out unrelated model errors (Flato et al., 2013, Otto-Bliesner et al. 2016)

60 and El Niño-Southern Oscillation (ENSO) effects (Iles et al., 2013, Stevenson et al. 2016). It
61 even enhances climate prediction skills (Kadow et al. 2015), which are significantly affected by
62 volcanic aerosols (Timmreck et al., 2016). Multi-model ensemble mean (MMEM) of the fifth
63 phase of Coupled Model Intercomparison Project (CMIP5) shows a large improvement in
64 reflecting global temperature and precipitation variation (Knutti & Sedláček, 2012; Flato et al.,
65 2013) as well as monsoon precipitation variation in East Asia (Song & Zhou, 2014; Kusunoki &
66 Arakawa, 2015). Using MMEM of CMIP5 model output, responses of reduced temperature and
67 summer monsoon rainfall to volcanic eruptions are also clearly detected in historical simulations
68 (Zambri & Robock, 2016), and even in the “last millennium (LM)” experiment of CMIP5
69 (Zambri et al, 2017).

70 The climate effect to volcanic eruptions reported in Zambri et al. (2017) is more about the
71 global scale. For future water management and coping strategy after volcanic perturbation, it’s
72 important to concentrate on the regional scale. With consideration on different dominated
73 subregions in the AMR, we compare proxy reconstruction and models in different subregions.
74 This study tries to answer following questions: what are the similarities and discrepancies
75 between proxy reconstruction and model on reflecting volcanic eruptions’ hydrological effects in
76 different subregions of the AMR? Are CMIP5 MMEMs able to reproduce volcanic eruptions’
77 hydrological effects in the AMR? Following here are data and methods in section 2; comparisons
78 of spatio-temporal hydrological patterns are presented in section 3; in section 4, we discuss the
79 uncertainty source; we present our conclusions to answer the referred questions in section 5.

80 2 Data and Methods

81 2.1 Proxy Data and Covered Subregions

82 The proxy reconstruction data we adopt is Monsoon Asia Drought Atlas (MADA, Cook
83 et al., 2010). It is a reconstruction of June-July-August (JJA) Palmer Drought Severity Index
84 (PDSI) based on tree ring chronologies and PDSI reconstruction data (Dai et al., 2004), which
85 has annual recordings from 1300 CE to 2005 CE and $2.5^\circ \times 2.5^\circ$ spatial resolution in the AMR.
86 Hereafter, I refer to MADA as MADA PDSI. The same as PDSI, positive MADA PDSI values
87 represent wet conditions while negative values stand for dry conditions. Drought emerges when
88 MADA PDSI falls below -0.5 while flood develops when it is over 0.5. It has been widely used
89 as a reference data set for proxy-model comparisons on volcanic eruptions' hydrological effects
90 in the AMR (Anchukaitis et al., 2010; Zhang et al., 2012; Wegmann et al., 2014, Stevenson et
91 al., 2016, 2017).

92 In previous studies, proxy-model comparisons between MADA PDSI and models were
93 conducted over the AMR (Anchukaitis et al., 2010; Wegmann et al., 2014; Stevenson et al.,
94 2016, 2017). No selection was made regarding regional difference of dominant climate and data
95 reliability. The AMR is not only dominated by monsoon climate, instead, different hydrological
96 conditions are shown on two sides of the modern Asian summer monsoon limit (red dashed line
97 in figure 1), to the northwest are the westerlies-dominated arid areas, whereas to the southeast
98 are the monsoon-dominated humid areas (Dando, 2005; Herzschuh, 2006; Chen et al., 2008). It
99 includes two monsoon subsystems - East Asian Summer Monsoon (EASM) and South Asian
100 Summer Monsoon (SASM), which are usually separated by 100°E longitude (Herzschuh, 2006;
101 Chiang et al., 2017). Considering this, we also performed time series analysis over the separated
102 westerlies and monsoon-dominated subregions.

103 For spatial comparisons, as shown in figure 1, locations of the available tree ring
104 chronologies (green dots) distribute irregularly over the AMR. This might cause different
105 reliability of the MADA PDSI in different areas. According to Asian geographical distribution
106 (Fan, 2017), the study area covers part of North Asia (NA), Central Asia (CA), and all the
107 countries in East Asia (EA), South Asia (SA) and Southeast Asia (SeA). Considering the two
108 monsoon systems, we separate the whole region into seven subregions (separated by purple
109 boundary lines in figure 1) for more detailed discussion. We can see that western-East Asia (w-
110 EA) is the subregion that has the most tree ring chronologies especially the ones dating back to
111 1300 CE (Cook et al., 2010). Among the monsoon-dominated subregions, SASM has more tree
112 ring chronologies, followed by EASM and SeA. Among westerlies-dominated subregions,
113 several tree ring chronologies are concentrated in the central part of North Asia (NA), most of
114 them only date back to 1700 CE (Cook et al., 2010); western-South Asia (w-SA) and Central
115 Asia (CA) have less tree ring sites.

116 **Figure 1.** The proxy reconstruction data MADA PDSI and the divided subregions. Modified
117 from figure 1 of Cook et al. (2010). Red crosses show the 534 grid points. Green dots indicate
118 the locations of the tree-ring chronologies. Seven subregions are divided by purple curves.
119 Dashed red line indicates the modern Asian summer monsoon limit after Chen et al. (2008).
120 Areas with yellow background indicate westerlies-dominated subregions: North Asia (NA),
121 Central Asia (CA), western-South Asia (w-SA); areas with light green background indicate

122 monsoon-dominated subregions: East Asian summer monsoon (EASM, east of 100°E after
123 Chiang et al. (2017)), South Asian summer monsoon (SASM) and Southeast Asia (SeA).
124 Western-East Asia (w-EA) is the monsoon-westerlies transition zone.

125 2.2 Model ensembles and volcanic classifications

126 The “LM” experiment of CMIP5 was performed only by nine modelling groups
127 performed the experiment (Schmidt et al., 2011). They can freely choose one of the two volcanic
128 forcing data sets - GRA (Gao et al., 2008) and CEA (Crowley & Unterman, 2013). We separate
129 models into two groups of MMEMs based on the adopted volcanic forcing data sets. To keep the
130 same number of ensemble members involved in the MMEMs, we adopt six ensemble members
131 of four models in each group, as shown in the green box in figure 2, more information about the
132 model ensemble members are listed in table s1. Only GISS-E2-R model has three ensemble
133 members, which might predominate the MMEM. Considering this, two set of MMEMs with four
134 ensemble members (in black in the green box of figure 2), including only one ensemble member
135 from GISS-E2-R, are tested. Two times of GRA volcanic forcing was used in the GISS-E2-R
136 model simulations. This exaggerated volcanic forcing might cause excessive climate effects in
137 the GRA-based group of CMIP5 MMEMs. To verify the model results, we also adopt all the
138 available five ensemble members of the “volcanic only” experiment from the Last Millennium
139 Ensemble (LME, Otto-Bliesner et al., 2016). This project performed large number of LM
140 simulations with CESM1 (CAM5) model (Hurrell et al., 2013). In the “volcanic only”
141 experiment, the GRA reconstruction (Gao et al., 2008) was adopted as the volcanic forcing
142 dataset. Other forcing including solar variability, land use, GHGs and orbital changes were fixed
143 to the same value as in 850 CE.

144 **Figure 2.** Volcanic years and northern hemisphere aerosol injection in GNH and CNH
145 classifications. Red lines indicate that the volcanic events are included in both classifications.
146 Model ensembles used in two classifications are shown in the green box, four model ensembles
147 in black were used in the test of another round of multi-model ensemble means.

148 Following Zhuo et al. (2014), we construct two classifications - GNH and CNH - based
149 on GRA and CEA volcanic forcing indices, with the chosen volcanic events that have larger
150 northern hemisphere sulfate injection than 1991 Pinatubo eruption. The same as in Zhuo et al.
151 (2014), for the events that without certain eruption date, we assume that they were erupted in
152 spring; for the eruptions that occurred after August, we adjusted the eruption year to the next
153 year, as their climatic impacts are likely to take effect during the next boreal summer. The
154 chosen volcanic events and related aerosol injection magnitude are shown in figure 2, and the
155 specific values are listed in table s2. MADA PDSI has recording in 1300-2005 CE, while CMIP5
156 “LM” experiment covers the period of 850-1849 CE. The overlapped period covering 1300-1849
157 CE were chosen as our core study period. In 1300-1849 CE, GNH classification has 12 volcanic
158 events while CNH classification has 18 events. Different number of classified events may lead to
159 different results between two classifications. We tested this uncertainty using classifications with
160 nine events that are included in both classifications (as shown in red in figure 2). In order to
161 verify the model results, analyses covering the whole period of 850-1849 CE are also made for
162 CMIP5 PDSI and LME PDSI.

163 2.3 Methods

164 For better comparison between proxy reconstruction and models, CMIP5 “LM”
165 experiment outputs are regridded to the same spatial resolution as MADA PDSI. Then, using the
166 MATLAB program produced by Jacobi et al. (2013), model precipitation and temperature data,
167 together with latitude and water-holding capacities (Webb et al., 2000), are transferred into
168 PDSI. Finally, the MMEM of PDSI is calculated. Hereafter, it’s referred to as CMIP5 PDSI.
169 Model ensemble members from LME have the same resolution. These model outputs are directly
170 transferred into PDSI, and the multi-member mean is referred to as LME PDSI in this study.

171 Considering that PDSI combines both temperature and precipitation, we also adopted
172 another widely used hydrological drought index: 12-months of Standardized Precipitation Index
173 (SPI12, Mckee et al., 1993), which transferred only from model precipitation data. It indicates
174 evident low water supply, especially in streams, reservoirs, and groundwater levels. This
175 indicates the societal impact of continuous meteorological drought. Negative and positive values
176 indicate specific drought and wet conditions. It indicates mild drought once SPI12 falls below
177 zero. The same as CMIP5 PDSI, MMEM of SPI12 from CMIP5 “LM” experiment is calculated
178 and referred to as CMIP5 SPI12. MADA PDSI only reflects the hydrological condition of the
179 boreal summer season. To keep model data the same as MADA PDSI, we analyze summer JJA
180 mean of CMIP5 PDSI and CMIP5 SPI12 in this study.

181 After pretreatment of the classifications and hydrological data, we conduct Superposed
182 Epoch Analysis (SEA, Haurwitz & Brier, 1981) on hydrological indices (MADA PDSI, CMIP5
183 PDSI, CMIP5 SPI12 and LME PDSI) for 11 years (-5 to 5) surrounding the eruption year (year
184 0) in each classification. To study the significance of the hydrological effects, we conduct Monte
185 Carlo model tests (Adams et al., 2003) based on the null hypothesis that there is no relationship
186 between volcanoes and hydrological conditions. Each volcanic event is randomly reassigned a
187 new eruption year in the study period, and then the average values of the hydrological indices are
188 calculated for the 11 years. For significance tests of time series analysis, 10000 times of
189 resampling are made on regional averaged hydrological indices. For spatial analyses, 1000 times
190 of resampling are made on each grid. This builds a random distribution, against which our SEA
191 results are considered to be statistically significant at the 95% (99%) confidence level when they
192 exceed the 95% (99%) range of the Monte Carlo results. To quantify the same drought and wet
193 areas between proxy and MMEMs, we counted the number of grid cells that have same sign
194 between MADA PDSI and CMIP5 PDSI/SPI12, then calculated their percentage in each
195 subregion.

196 **3 Comparison of spatio-temporal hydrological patterns**

197 3.1 Temporal hydrological responses to volcanic classifications

198 Figure 3 shows the SEA results of MADA PDSI, CMIP5 PDSI and CMIP5 SPI12 over
199 the Asian monsoon region for GNH and CNH volcanic classifications. As shown in figure 3a,
200 MADA PDSI decreases in one year after the eruption (year 1), and significant drying effect
201 emerges in two and three years after the eruption (year 2 and year 3). CMIP5 PDSI decreases
202 promptly and sharply in the eruption year (year 0). The significant drying effects last for three
203 years, and gradually recover to normal condition in year 4. Similarly, CMIP5 SPI12 decreases

204 rapidly in year 0 and year 1, after the strongest drying effects in year 1, it gradually recovers in
 205 year 2 and turns to normal condition in year 3. This indicates an agreement between MADA
 206 PDSI and CMIP5 PDSI/SPI12 on the drying effects of the volcanic eruptions, although with one
 207 year of time lag in MADA PDSI compared to CMIP5 PDSI/SPI12, and the magnitude shown in
 208 CMIP5 PDSI/SPI12 are much larger than that in MADA PDSI. This is probably due to
 209 exaggerated two times of the GRA forcing used in the GISS-E2-R model simulations. Figure 3b
 210 shows hydrological responses to the CNH volcanic eruptions. The response tendency is similar
 211 to that in the GNH classification, MADA PDSI increases before the eruption, and decreases in
 212 year 1 and year 2; CMIP5 PDSI and CMIP5 SPI12 decreases promptly in year 0 and reach the
 213 lowest value in year 1, then gradually recovers from year 2. Comparing to the significant results
 214 (even at the 99% confidence level) in the GNH classification, the results are less significant in
 215 the CNH classification, but the magnitudes between MADA PDSI and CMIP5 PDSI/SPI12 are
 216 closer to each other. The different scale between MEMs of two classifications might also result
 217 from different number of superposed volcanic events. But differences still exist when the
 218 classifications are constructed only with the same nine events in both volcanic forcing indices
 219 (shown in red in figure 2). Crowley et al. (2013) suggested that volcanic forcing in the GRA
 220 index is overestimated. When reconstructing the CEA index, they used a scaling of two-thirds to
 221 calculate the forcing of the explosive eruptions which are larger than 1991 Pinatubo eruption.
 222 Volcanic events included in the CNH classification are affected by this scaling process, which
 223 result in the minor hydrological responses.

224 **Figure 3.** Temporal SEA results of MADA PDSI (blue lines), JJA mean CMIP5 PDSI (red lines)
 225 and CMIP5 SPI12 (pink lines) corresponding to GNH (a) and CNH (b) volcanic classifications in
 226 1300-1850 CE over the Asian monsoon region. The thinner lines stand for the relative Monte
 227 Carlo model results at the 95% confidence level. The asterisks represent the year that passed the
 228 Monte Carlo model tests at the 99% confidence level. Year 0 represents the identified eruption
 229 year by volcanic forcing indices, negative and positive years represent relative years before and
 230 after the eruption.

231 **Figure 4:** Same as figure 3 but for LME PDSI in 1300-1849 CE, and both LME PDSI and
 232 CMIP5 PDSI in 850-1849 CE.

233 The exaggerated two times-GRA forcing used in the GISS-E2-R model simulations also
 234 cause the excessive climate response in the GNH classification. As shown in figure 4, temporal
 235 SEA results of LME PDSI over two periods show significant drying effects in year 0 and the
 236 significant drying effects last to year 1. CMIP5 PDSI shows excessive drying effects over the
 237 whole period, which is similar to that shown in figure 3a over the core study period. This
 238 confirms the findings shown in Zhuo et al. (2014) that larger volcanic aerosol magnitude leads to
 239 larger drying effect. The significant drying effects in two to three years after the volcanic
 240 eruptions agree with previous research findings (Anchukaitis et al., 2010; Man et al., 2014; Zhuo
 241 et al., 2014; Liu et al, 2016), which is prominent in the general background of a significant
 242 reduction in global precipitation (Iles & Hegerl, 2014).

243 Temporal SEA analysis over the whole region confound the different climate conditions
 244 in the westerlies and monsoon-dominated subregions. Additionally, temporal SEA results over
 245 the separated westerlies and monsoon-dominated subregions are presented. Figure 5a shows
 246 different hydrological responses in the WDSR, as MADA PDSI in both the GNH (solid blue

247 line) and CNH (dotted blue line) classifications increase from the negative in year -3 to the
 248 positive in year -2. The wet conditions extend to in year 0 to year 2, then turn to dry conditions in
 249 year 3 to year 5. MADA PDSI in year 1 and year 2 in the CNH classification pass the
 250 significance test, but only at the 95% confidence level, and the values do not exceed the largest
 251 value in year -5 and the smallest value in year 5. This might indicate that the hydrological
 252 response to volcanic perturbations in the WDSR is insensitive to volcanic forcing. However,
 253 CMIP5 PDSI and CMIP5 SPI12 in the GNH classification show highly significant drying effects
 254 in year 0 to year 3 at the 99% confidence level. In the CNH classification, CMIP5 SPI12 shows
 255 significant drying effects in year 1 and year 2, but CMIP5 PDSI does not indicate drying effect,
 256 instead only significant wetting variation are shown in year -1. This indicates a large difference
 257 between MADA PDSI and CMIP5 PDSI/SPI12 in the WDSR. Considering the exaggerated
 258 volcanic forcing used in the GNH classification, this might suggest that the wetting or drying
 259 effect in this insensitive area depends largely on the magnitude of the injected volcanic aerosols.
 260 In the MDSR (figure 5b), MADA PDSI and CMIP5 PDSI/SPI12 in two classifications all agree
 261 on the drying effects in year 0 and year 1, and the recovering from year 2 onwards. We note that
 262 the time-lag effect of proxy data probably exists. As MADA PDSI decreases in year 0, but the
 263 significant drying effects are shown in year 1, whereas, CMIP5 PDSI/SPI12 show a sharp
 264 decrease in year 0 and the significant drying effects extend to year 1.

265 **Figure 5:** Temporal SEA results of MADA PDSI (blue lines), JJA mean CMIP5 PDSI (red lines)
 266 and CMIP5 SPI12 (pink lines) corresponding to GNH (solid lines) and CNH (dashed lines)
 267 volcanic classifications in 1300-1850 CE over the westerlies-dominated subregion (a) and
 268 monsoon-dominated subregion (b). Small and large circle dots indicate the years are significant
 269 at the 95% and 99% confidence level.

270 Figure 6 shows the temporal SEA results of LME PDSI over both periods and CMIP5
 271 PDSI over the whole period over the separated westerlies and monsoon-dominated subregions.
 272 In the WDSR, CMIP5 PDSI indicates significant drying effects over the whole period (850-
 273 1849). LME PDSI increases in year 1 and decreases from year 2 to year 5 over both periods. This
 274 is similar to the response tendency of MADA PDSI in the GNH classification (figure 5a), but
 275 both results did not pass the significance tests even at the 95% confidence level. In the MDSR,
 276 model results all suggest consistent drying effects in the year 0 and year 1, and then gradually
 277 recover in year 2.

278 **Figure 6:** Same as figure 5 but for LME PDSI in 1300-1849 CE, and both LME PDSI and
 279 CMIP5 PDSI in 850-1849 CE.

280 3.2 Spatial patterns of the hydrological response

281 Considering uncertainties of spatial responses arising from the estimated aerosol magnitude
 282 in volcanic forcing reconstructions, following discussions focus on horizontal distribution of the
 283 hydrological tendencies. To quantify the similarity of drought and wet areas between proxy and
 284 model, in figure 7, we show percentages of grid cells that have same sign between MADA PDSI
 285 and CMIP5 PDSI/SPI12 in different subregions in year 0 (in magenta) and year 1 (in red). When
 286 separated into two dominated subregions, it is hard to find out consistent variation tendency,
 287 except that the percentage increases from year 0 to year 1 in the WDSR while decreases in the
 288 MDSR, and different ensemble members show larger difference in the WDSR than in the MDSR.

289 When separated into seven subregions with consideration of the spatial coverage of tree ring
 290 chronologies, the percentages show large differences in different subregions. Four subfigures all
 291 indicate that the largest similarity between MADA PDSI and CMIP5 PDSI/SPI12 emerges in the
 292 w-EA, where the most tree ring chronologies are available, in both year 0 and year 1. It also
 293 shows fewest difference among different ensemble members. Single model and MADA PDSI
 294 have large uncertainty. The consistency among different groups and ensemble members improve
 295 the reliability of reflecting the hydrological effects of volcanic eruptions by both proxy and
 296 models. Better agreements are then shown in SASM and EASM, with less difference among
 297 different ensemble members than in w-SA and SeA. These results suggest that proxy and models
 298 agree better in the subregions with more tree ring chronologies, which indicates an important
 299 role the available tree ring chronology plays on the reliability of proxy reconstruction data. The
 300 percentages are mainly larger in year 1 than in year 0, except for NA and CA, where have the
 301 fewest tree ring chronologies. This is consistent with the temporal SEA results, and spatially
 302 quantify that MADA PDSI and CMIP5 MEMs agree better in monsoon-dominated subregions
 303 in year 1.

304 **Figure 7:** Histogram on percentages of grid cells that have same sign between MADA PDSI and
 305 CMIP5 PDSI/SPI12 in the GNH classification (a/b) and CNH classification (c/d). Columns
 306 indicate the percentages in the westerlies-dominated subregion (WDSR) and monsoon-
 307 dominated subregion (MDSR) as well as in the seven subregions in year 0 (in magenta) and year
 308 1 (in red). Different marks indicate the percentages between MADA PDSI and PDSI/SPI12 of
 309 different single ensemble members.

310 **Figure 8:** Spatial response of MADA PDSI (a), JJA mean CMIP5 PDSI (b) and CMIP5 SPI12
 311 (c) to GNH volcanic classification in 1300-1850 CE in the Asian monsoon region. The grid cells
 312 marked by black dots and slashes denote areas that passed the Monte Carlo model significance
 313 tests at the 95% and 99% confidence levels. Year 0 represents the volcanic eruption year by
 314 volcanic forcing indices, negative and positive years represent relative years before and after the
 315 eruption.

316 To investigate the spatial distribution of the hydrological variation, we show the spatial
 317 patterns of the superposed hydrological responses to the GNH classification in figure 8. CMIP5
 318 PDSI (figure 8b) shows drier conditions before the eruption (Year -5 to -1 ave) than that in
 319 MADA PDSI (figure 8a), but with a similar southeast-wet-northwest-dry dipolar distribution.
 320 MADA PDSI shows wet conditions in NA, northeast EASM and SeA in year 0 and in CA in
 321 year 1. However, most results do not pass the significance test. Significant drying effects develop
 322 in w-EA in year 0 and extends to SASM and northern EASM in year 1; the drying effects are
 323 reflected by the disappearance of the wet areas in SeA. Consistent with the temporal SEA results,
 324 MADA PDSI shows the strongest effect in year 1, with drying effects in monsoon-dominated
 325 subregions and wetting effects in westerlies-dominated subregions. This gradually reverses in
 326 year 2 and turns to wet in the monsoon-dominated subregions while drought in the westerlies-
 327 dominated subregions in year 3. Comparing to MADA PDSI, CMIP5 PDSI shows faster and
 328 longer effects, with overall significant drying effects in year 0 to year 2 at the 99% confidence
 329 level, except for the wet areas in w-SA and southern EASM. Similarly, drought areas in the
 330 monsoon-dominated subregions turn to wet in year 3, while drying effects maintain in the
 331 westerlies-dominated subregions (figure 8b). These patterns are well verified by CMIP5 SPI12,
 332 which displays similar patterns in figure 8c. From the hydrological variation tendency, proxy-

333 model comparisons suggest similar drying to wetting variation in monsoon-dominated
 334 subregions (EASM, SASM and SeA), with faster and longer effects shown in the models than in
 335 the proxy data. This might result from the excessive volcanic forcing used in the GISS-E2-R
 336 model simulations. The ecological time lag-effect of the tree-ring based proxy reconstruction
 337 (Wu et al., 2005) and the dating uncertainty of volcanic eruption might also contribute to the
 338 difference. General agreements are shown in w-EA, where has a dense coverage of tree ring
 339 chronologies. In the westerlies-dominated subregions with rare tree rings, MADA PDSI shows
 340 wetting to drying transitions, CMIP5 PDSI/SPI12 show continuous drying effects in CA and NA,
 341 but wetting effects in w-SA. This is consistent with the temporal SEA results shown in figure 5,
 342 that MADA PDSI and CMIP5 PDSI/SPI12 agree on the tendency of the hydrological response to
 343 volcanic perturbation in the MDSR, while discrepancies exist in the WDSR.

344 In the CNH classification (figure 9), MADA PDSI (figure 9a) and CMIP5 PDSI (figure
 345 9b) indicate weaker effects of volcanic perturbations. It shows similar hydrological patterns as
 346 that in the GNH classification (figure 8a and 8b), except that CMIP5 PDSI shows limited
 347 response in CA and NA (figure 9b). The drying effects shown in the GNH classification (figure 8
 348 (b)) might be caused by the response to the exaggerated volcanic forcing used in GISS-E2-R
 349 model simulations. CMIP5 SPI12 (figure 9c) indicates even weaker effects, but the obvious
 350 drought areas agree well with those CMIP5 PDSI patterns. Better agreement between MADA
 351 PDSI and CMIP5 PDSI/SPI12 occurs in the subregions with more available tree ring
 352 chronologies. Highly significant results of CMIP5 PDSI/SPI12 in the GNH and CNH
 353 classifications indicate the consistency of MEMs on reproducing volcanic aerosols'
 354 hydrological effects in southern AMR. In CA and NA, discrepancies between MADA PDSI and
 355 CMIP5 PDSI/SPI12 do not allow drawing definite conclusions.

356 To verify model results, we show spatial patterns of LME PDSI over both periods (1300-
 357 1849 and 850-1849) and CMIP5 PDSI over the whole period (850-1849) in figure 10, CMIP5
 358 PDSI shows similar patterns even when extending the period to the whole 1000 years (figure
 359 10c). Similar patterns are also shown in LME PDSI over both periods, especially in southern
 360 Asian monsoon region. The drought and wet areas are not totally same among these different
 361 model results. However, with different model resolutions, it is fastidious to have complete
 362 matches. This indicates that the study periods, the number of the superposed events and the
 363 aerosol magnitude do not affect much the spatial patterns of the hydrological effects. These
 364 similar patterns support the reliability of models on reproducing the hydrological effects of
 365 volcanic eruptions in southern Asian monsoon region. LME PDSI also suggest slight drying
 366 effect in NA from year 0 to year 2 over both periods. These PDSI patterns might suggest that
 367 drying effects can emerge in NA and CA with strong enough volcanic forcing.

368 **Figure 9:** Same as figure 8 but response to CNH volcanic classification.

369 Summarizing the proxy-model comparison on the spatio-temporal patterns of
 370 hydrological responses to volcanic eruptions, one finds similar drying effects in the MDSR while
 371 discrepancies exist in the WDSR. Results show a better agreement on the spatial patterns in w-
 372 EA, SASM and EASM where there are more available tree ring chronologies. This poses an
 373 advance on previous studies. Anchukaitis et al. (2010) showed an east-dry-west-wet dipolar
 374 pattern by single model CSM1.4. Zhang et al. (2012) showed wetting effects in central Asia by
 375 ensemble mean of single model MPI-COSMOS. MADA PDSI shows different spatial pattern

376 (Anchukaitis et al., 2010; Zhang et al., 2012). Stevenson et al. (2016, 2017) also showed
 377 different patterns between MADA PDSI and ensemble mean of single model CESM. These
 378 spatial comparisons were made only in the eruption year. In comparison, our results were based
 379 on MMEMs and showed significant improvements. Spatial comparisons of three years are
 380 presented and suggest a better agreement in year 1 than in year 0. CMIP5 PDSI and CMIP5
 381 SPI12 verify each other between two classifications with highly significant results. Similar
 382 spatial patterns of LEM PDSI indicate the reliability of model simulations. They agree better in
 383 the monsoon-dominated subregions with MADA PDSI responding to volcanic eruptions. In the
 384 southern Asian monsoon region, spatial patterns of MMEMs in year 0 and year 1 agree well with
 385 precipitation anomaly pattern after Krakatau and Pinatubo eruptions shown in Zambri and
 386 Robock (2016). The identified wet areas in EASM are close to that in Gao and Gao (2018),
 387 which showed an increased precipitation over the Yangtze-Huaihe River valley using Feng et al.
 388 (2013) precipitation reconstruction. The patterns are also consistent with the observed
 389 precipitation and PDSI variations shown in Trenberth and Dai (2007), with a drying effect in
 390 SASM, SeA and northern EASM, and wetting effect in w-SA and southern EASM after the
 391 Mount Pinatubo eruption. In the northern Asian monsoon region, except for PDSI, which suggest
 392 drying effects (Trenberth and Dai, 2007), limited effects are shown in precipitation (Trenberth
 393 and Dai, 2007; Zambri and Robock, 2016) and runoff variations (Trenberth and Dai, 2007).
 394 These results indicate the reliability of MMEMs in reflecting the spatio-temporal patterns of
 395 hydrological response to volcanic perturbations in the Asian monsoon region, except for Central
 396 Asia and North Asia; one cannot draw definite conclusion in these two subregions, because
 397 CMIP5 PDSI and CMIP5 SPI12 in the CNH classification display no impact, and there are
 398 limited available observations in these subregions to validate the results.

399 **Figure 10:** Same as figure 8 but for LME PDSI in 1300-1849 CE, and both LME PDSI and
 400 CMIP5 PDSI in 850-1849 CE.

401 **4 Discussion on uncertainty source**

402 Results suggest large discrepancy between MADA PDSI and models in the westerlies-
 403 dominated subregions with fewer available tree ring chronologies. It suggests a better agreement
 404 in one year after the eruption instead of in the eruption year. These discrepancies indicate the
 405 uncertainty of the results deriving from the data source and analysis process. As suggested by
 406 PAGES Hydro2k Consortium (2017), we treat proxy reconstruction and model data equally, and
 407 discuss uncertainties and limitations of both MADA PDSI and CMIP5 PDSI/SPI12. From the
 408 temporal SEA results of the Asian monsoon region (figure 3), we can see that CMIP5
 409 PDSI/SPI12 agrees with MADA PDSI on the drying effects of explosive volcanic eruptions.
 410 CMIP5 PDSI shows stronger effects than MADA PDSI in the GNH classification. Stronger
 411 effects are also shown in the GNH classification than that in the CNH classification. This is
 412 caused by both the exaggerated volcanic forcing used in the GISS-E2-R model ensemble
 413 members and the reduced amplitude of the forcing in the CEA reconstruction (Crowley et al.,
 414 2008, 2013). This can be verified by the results of LME PDSI. Besides, faster responses are
 415 shown in CMIP5 PDSI/SPI12 than that in MADA PDSI in both classifications. This reflects the
 416 time lag effect in the tree-ring-based ecological response compared to the meteorological
 417 response in the model simulation (Wu et al., 2005).

418 Volcanic years identified in volcanic forcing indices deviate from the reality. Superposed

419 volcanic classification averages out the effect of single event, but the dating uncertainty of
420 volcanic events can cause large uncertainty on the hydrological effects reflected by MADA
421 PDSI. Uncertainty of eruption month coming from the volcanic forcing indices also bring
422 uncertainty on defining the eruption year. This might explain the abnormal wetting effect in year
423 0 shown by MADA PDSI (figure 3), which was also identified in Anchukaitis et al. (2010) after
424 different superposed volcanic events. To investigate these uncertainties, we test several different
425 classifications. Volcanic years and the number of included events in different classifications are
426 listed in table s3. We show response of MADA PDSI to these different classifications in figure
427 11. The same as in the GNH and CNH classifications, MADA PDSI suggests wetting effects in
428 year 0 in the GCNH classification. However, MADA PDSI starts to decrease in year 0, and drops
429 to the lowest value in year 2 and year 3 in SNH and A07 classifications, respectively. SNH
430 classification is based on the most start-of-the-art volcanic forcing reconstruction, which largely
431 improved the dating accuracy (Sigl et al., 2015), while A07 classification includes only those
432 five explosive eruptions that are the most well-known events during the past centuries. These
433 two classifications have minimum dating uncertainty among the volcanic classifications used in
434 this study. This indicates that the dating uncertainty largely affect the climate response especially
435 in year 0. The wetting effects shown by MADA PDSI are probably result from dating uncertainty
436 of the volcanic events.

437 **Figure 11:** Temporal SEA results of MADA PDSI corresponding to different classifications of
438 volcanic eruptions.

439 The temporal SEA results of two separated subregions (figure 5) suggest an agreement
440 between MADA PDSI and CMIP5 PDSI/SPI12 in the MDSR while large discrepancies exist in
441 the WDSR. Quantification of the grid cells with same sign between MADA PDSI and CMIP5
442 PDSI/SPI12 indicates a better agreement in subregions with more tree ring chronologies and in
443 the second summer after the volcanic perturbations. This might explain partly the spatial proxy-
444 model discrepancies suggested by precious studies (Anchukaitis et al., 2010; Zhang et al., 2012;
445 Stevenson et al., 2016, 2017), because comparisons were only made in the first summer after the
446 eruptions. Comparisons on spatial patterns of the hydrological effects show large discrepancies
447 in westerlies-dominated subregions with limited tree ring chronologies. This reveals the
448 limitation of MADA PDSI caused by the spatial coverage of tree ring chronologies. The drying
449 tendencies in NA and CA reflected by CMIP5 PDSI/SPI12 in the GNH classification might be
450 realistic, but it might be misleading patterns coming from the exaggerated volcanic forcing used
451 in the GISS-E2-R model ensemble members. This exaggerated forcing also contributes to the
452 faster and longer drying effects of volcanic perturbation in monsoon-dominated subregions.

453 Spatial SEA results (figure 8) indicate significant wetting effects in NA by MADA PDSI,
454 which are opposite to the drying effects shown by CMIP5 PDSI and LME PDSI in the GNH
455 classification. Similar discrepancies were also presented in Liu et al. (2016). This may indicate
456 data uncertainties of MADA PDSI, especially in westerlies-dominated subregions where are
457 short of tree ring chronologies that go back to 1300 CE (Cook et al., 2010). However, we would
458 like to point out that the models also suggest wetting effects in the western areas, and the wet
459 areas vary a bit in different groups of model ensemble means, which have different forcing
460 magnitudes. Thus, the discrepancies can be also caused by the uncertain aerosol magnitudes and
461 the consequent uncertain effects shown in the models. The difference in resolution of both proxy
462 reconstruction and models also introduces uncertainties.

463 A limited number of ensemble members might bring uncertainty to the model results.
464 Especially, three ensemble members of GISS-E2-R model might have a predominant effect on
465 the MMEMs. However, when testing MMEMs with only four members (members in black in
466 figure 2), which include only one member of GISS-E2-R model, temporal and spatial patterns
467 remain largely unchanged. Deviation of the model-based analysis between two classifications
468 can come from the number of classified events based on volcanic forcing indices. When testing
469 the classifications with the same nine events in both indices (marked in red in figure 2), temporal
470 and spatial patterns remain largely constant.

471 The internal variability of the climate system often brings uncertainty on detecting the
472 hydrological effects of volcanic eruptions, especially the hardly constrained effects of the
473 concurrent ENSO events (Adams et al., 2003; Li et al., 2013; khodri et al., 2017; Stevenson et
474 al., 2016, 2017). The effect of eruption seasons on the circulation and ENSO can bring extra
475 uncertainties (Stevenson et al., 2017). All these might contribute to the proxy-model
476 discrepancies, especially in the initial phase and the phase-out period of the hydrological effects.
477 Following the method in Iles et al. (2013), we test this uncertainty through repeating the SEA
478 analysis after regressing out the effect of ENSO. Consistent with Iles et al. (2013) and Iles and
479 Hegerl (2014), it only results in a lower response in amplitude, but the temporal and spatial
480 patterns remain largely unchanged. In addition, previous researches show that volcanic eruptions
481 can affect the hydrological condition through affecting the evolution of ENSO in time, but with
482 large contradictory findings (Adams et al., 2003; Li et al., 2013; Stevenson et al., 2016; Wang et
483 al., 2017; Liu et al., 2018; Sun et al., 2018). This is an additional source contributing to proxy-
484 model discrepancies. Future improvement of volcanic forcing reconstructions, model
485 simulations, proxy reconstructions and observations will lead to a better understanding and
486 reconciling the proxy-model discrepancies.

487 **5 Conclusions**

488 Previous studies show large discrepancies between proxy and model on volcanic
489 aerosols' hydrological response patterns in the Asian monsoon region. In this study, we use tree
490 ring-based proxy data MADA PDSI and a number of model ensemble members from CMIP5 and
491 LME, to compare their spatio-temporal hydrological response to two classified volcanic events
492 in 1300 – 1850 CE in subregions of monsoon Asia.

493 Our temporal SEA results show that MADA PDSI and models agree on the significant
494 drying effects of volcanic aerosols in the MDSR, while disagreement exists in the WDSR.
495 Spatial comparisons indicate better agreement in subregions with more available tree ring
496 chronologies. Especially in w-EA, where has the most available tree ring chronologies dating
497 back to 1300 or even earlier, MADA PDSI agrees with models on the significant drying effects
498 of volcanic aerosols. In monsoon-dominated subregions, MADA PDSI and models show similar
499 drying to wetting variations after the volcanic perturbations, with rapider and prolonged drying
500 effects shown by models, which might result from the overestimated aerosol magnitude in the
501 volcanic forcing index and the time-lag effect of tree ring-based proxy reconstruction data. The
502 effect of uncertain eruption season on the circulation and the definition of the eruption year
503 might also contribute to their difference. Because of these uncertainties, MADA PDSI and
504 models show better consistency in year 1, with significant drying effects in northern EASM,
505 SASM and SeA, and opposite wetting effects in southern EASM. In westerlies-dominated

506 subregions, where lack of tree ring chronologies, MADA PDSI and models show larger
 507 discrepancies. Since two groups of CMIP5 MMEMs and LME PDSI all shows similar patterns,
 508 and with verification from previous studies, we propose the reliability of CMIP5 MMEMs on
 509 reflecting the wetting effects in w-SA. In CA and NA subregions, MADA PDSI shows
 510 significant wetting effects. CMIP5 MMEMs in GNH show significant drying effects, LME PDSI
 511 shows some drying effects only in NA, whereas CMIP5 MMEMs in CNH show limited
 512 response. Considering the lack of cross-verification, we do not draw certain conclusion in these
 513 two subregions.

514 Through spatio-temporal comparisons, we exam the reliability of MADA PDSI and
 515 CMIP5 MMEMs on reflecting the patterns of hydrological responses to volcanic perturbations. It
 516 suggests larger reliability of MADA PDSI in subregions with more available tree ring
 517 chronologies. Comparisons between proxy, observation and models indicate that CMIP5
 518 MMEMs are reliable to reflect the hydrological effects of volcanic aerosols in southern Asian
 519 monsoon region. Further analysis on CMIP6 and improved proxy reconstruction data will
 520 contribute to verify these results better.

521 This study discusses the long-standing proxy-model discrepancy problem. We treat the
 522 uncertainties and limitations of both proxy and models equally. This contributes to better
 523 interpretations on the results, and shed new light on the reliability of both proxy data and CMIP5
 524 model simulations on reflecting the hydrological effects of historical volcanic eruptions in Asian
 525 subregions. This might promote further researches like mechanism exploration that based highly
 526 on model simulations, which is important for better evaluating effects of both historical and
 527 future volcanic eruptions and feasibility of future choices on stratospheric aerosol injection
 528 engineering.

529 **Acknowledgments**

530 This work is supported by China Scholarship Council (CSC). The authors acknowledge the
 531 climate modelling groups listed in figure 1 and the Last Millennium Ensemble project group for
 532 producing and making their model outputs available, and the German Climate Computing Center
 533 (DKRZ, <https://www.dkrz.de/>) for making the CMIP5 model output and the computational
 534 resources available. CMIP5 model outputs are downloaded from [https://esgf-](https://esgf-data.dkrz.de/search/cmip5-dkrz/)
 535 [data.dkrz.de/search/cmip5-dkrz/](https://esgf-data.dkrz.de/search/cmip5-dkrz/). LME model outputs are downloaded from
 536 [https://www.earthsystemgrid.org/dataset/ucar.cgd.cesm4.CESM_CAM5_LME.atm.proc.monthly](https://www.earthsystemgrid.org/dataset/ucar.cgd.cesm4.CESM_CAM5_LME.atm.proc.monthly_ave.html)
 537 [_ave.html](https://www.earthsystemgrid.org/dataset/ucar.cgd.cesm4.CESM_CAM5_LME.atm.proc.monthly_ave.html). We thank Kirstin Krüger and Claudia Timmreck for helpful discussions.

538 **References**

- 539 Adams, J. B., Mann, M. E., & Ammann, C. M. (2003). Proxy evidence for an El Niño-like
 540 response to volcanic forcing. *Nature*, 426(6964), 274-278. doi:10.1038/nature02101
- 541 Anchukaitis, K. J., Buckley, B. M., Cook, E. R., Cook, B. I., D'Arrigo, R. D., & Ammann, C. M.
 542 (2010). Influence of volcanic eruptions on the climate of the Asian monsoon region. *Geophysical*
 543 *Research Letters*, 37(22), L22703. doi:10.1029/2010gl044843

- 544 Chen, F., Yu, Z., Yang, M., Ito, E., Wang, S., Madsen, D. B., et al. (2008). Holocene moisture
545 evolution in arid central Asia and its out-of-phase relationship with Asian monsoon history.
546 *Quaternary Science Reviews*, 27(3-4), 351-364. doi:10.1016/j.quascirev.2007.10.017
- 547 Chiang, J. C. H., Swenson, L. M., & Kong, W. (2017). Role of seasonal transitions and the
548 westerlies in the interannual variability of the East Asian summer monsoon precipitation.
549 *Geophysical Research Letters*, 44(8), 3788-3795. doi:10.1002/2017gl072739
- 550 Cook, E. R., Anchukaitis, K. J., Buckley, B. M., D'Arrigo, R. D., Jacoby, G. C., & Wright, W. E.
551 (2010). Asian monsoon failure and megadrought during the last millennium. *Science*, 328(5977),
552 486-489. doi:10.1126/science.1185188
- 553 Crowley, T. J., & Unterman, M. B. (2013). Technical details concerning development of a 1200
554 yr proxy index for global volcanism. *Earth System Science Data*, 5(1), 187-197.
555 doi:10.5194/essd-5-187-2013
- 556 Dai, A. G., Trenberth, K. E., & Qian, T. T. (2004). A global dataset of Palmer Drought Severity
557 Index for 1870–2002: Relationship with soil moisture and effects of surface warming, *Journal of*
558 *Hydrometeorology*, 5(6), 1117–1130.
- 559 Dando, W. A. (2005). Asia, climate of Siberia, Central and East Asia. *Encyclopedia of Earth*
560 *Sciences Series*. Dordrecht: Springer. https://doi.org/10.1007/1-4020-3266-8_19
- 561 Dufresne, J. L., Foujols, M. A., Denvil, S., Caubel, A., Marti, O., Aumont, O., et al. (2013).
562 Climate change projections using the IPSL-CM5 Earth System Model: from CMIP3 to CMIP5.
563 *Climate Dynamics*, 40(9-10), 2123-2165. doi:10.1007/s00382-012-1636-1
- 564 Fan, J. (Ed.). (2017). *Geography in the second volume of seventh grade*. Beijing: People's
565 Education.
- 566 Feng, S., Hu, Q., Wu, Q., & Mann, M. E. (2013). A Gridded Reconstruction of Warm Season
567 Precipitation for Asia Spanning the Past Half Millennium. *Journal of Climate*, 26(7), 2192-2204.
568 doi:10.1175/jcli-d-12-00099.1
- 569 Flato, G., J., Marotzke, B., Abiodun, P., Braconnot, S.C., Chou, W., Collins, P., et al. (2013).
570 Evaluation of climate models. In Stocker, T.F., Qin, D., Plattner, G. K., Tignor, M., Allen, S.K.,
571 Boschung, J. et al. (Eds.), *Climate Change 2013: The Physical Science Basis. Contribution of*
572 *Working Group I to the Fifth Assessment Report of the Intergovernmental Panel on Climate*
573 *Change* (pp. 741-866), Cambridge: Cambridge University
- 574 Gao, C., & Gao, Y. (2018). Revisited Asian Monsoon Hydroclimate Response to Volcanic
575 Eruptions. *Journal of Geophysical Research*, 123, 7883-7896. doi:10.1029/2017JD027907
- 576 Gao, C., Robock, A., & Ammann, C. (2008). Volcanic forcing of climate over the past 1500
577 years: An improved ice core-based index for climate models. *Journal of Geophysical Research*,
578 113(23), D23111. doi:10.1029/2008jd010239
- 579 Gent, P. R., Danabasoglu, G., Donner, L. J., Holland, M. M., Hunke, E. C., Jayne, S. R., et al.

- 580 (2011). The Community Climate System Model Version 4. *Journal of Climate*, 24(19), 4973-
581 4991. doi:10.1175/2011jcli4083.1
- 582 Giorgetta, M. A., Jungclaus, J., Reick, C. H., Legutke, S., Bader, J., Böttinger, M., et al. (2013).
583 Climate and carbon cycle changes from 1850 to 2100 in MPI-ESM simulations for the Coupled
584 Model Intercomparison Project phase 5. *Journal of Advances in Modeling Earth Systems*, 5(3),
585 572-597. doi:10.1002/jame.20038
- 586 Haurwitz, M. W., & Brier, G. W. (1981). A critique of the superposed epoch analysis method -
587 Its application to solar weather relations. *Monthly Weather Review*, 109(10), 2074–2079.
- 588 Herzsuh, U. (2006). Paleo-moisture evolution in monsoonal Central Asia during the last
589 50,000 years. *Quaternary Science Reviews*, 25(1-2), 163-178.
590 doi:10.1016/j.quascirev.2005.02.006
- 591 Iles, C. E., & Hegerl, G. C. (2014). The global precipitation response to volcanic eruptions in the
592 CMIP5 models. *Environmental Research Letters*, 9(10), 104012. doi:10.1088/1748-
593 9326/9/10/104012
- 594 Iles, C. E., Hegerl, G. C., Schurer, A. P., & Zhang, X. (2013). The effect of volcanic eruptions on
595 global precipitation. *Journal of Geophysical Research: Atmospheres*, 118(16), 8770-8786.
596 doi:10.1002/jgrd.50678
- 597 Jacobi, J., Perrone, D., Duncan, L. L., & Hornberger, G. (2013). A tool for calculating the
598 Palmer drought indices. *Water Resources Research*, 49(9), 6086-6089. doi:10.1002/wrcr.20342
- 599 Kadow, C., Illing, S., Kunst, O., Rust, H. W., Pohlmann, H., Müller, W. A., & Cubasch, U.
600 (2015). Evaluation of forecasts by accuracy and spread in the MiKlip decadal climate prediction
601 system. *Meteorologische Zeitschrift*. doi:10.1127/metz/2015/0639
- 602 Khodri, M., Izumo, T., Vialard, J., Janicot, S., Cassou, C., Lengaigne, M., et al. (2017). Tropical
603 explosive volcanic eruptions can trigger El Nino by cooling tropical Africa. *Nature*
604 *Communications*, 8(1), 778. doi:10.1038/s41467-017-00755-6
- 605 Kirchner, I., Stenchikov, G. L., Graf, H.-F., Robock, A., & Antuña, J. C. (1999). Climate model
606 simulation of winter warming and summer cooling following the 1991 Mount Pinatubo volcanic
607 eruption. *Journal of Geophysical Research: Atmospheres*, 104(D16), 19039-19055.
608 doi:10.1029/1999jd900213
- 609 Knutti, R., & Sedláček, J. (2012). Robustness and uncertainties in the new CMIP5 climate model
610 projections. *Nature Climate Change*, 3(4), 369-373. doi:10.1038/nclimate1716
- 611 Kusunoki, S., & Arakawa, O. (2015). Are CMIP5 models better than CMIP3 models in
612 simulating precipitation over East Asia? *Journal of Climate*, 28(14), 5601-5621.
613 doi:10.1175/jcli-d-14-00585.1

- 614 Li, J., Xie, S. P., Cook, E. R., Morales, M. S., Christie, D. A., Johnson, N. C., et al. (2013). El
615 Niño modulations over the past seven centuries. *Nature Climate Change*, 3(9), 822-826.
616 doi:10.1038/nclimate1936
- 617 Liu, F., Chai, J., Wang, B., Liu, J., Zhang, X., & Wang, Z. (2016). Global monsoon precipitation
618 responses to large volcanic eruptions. *Sci Rep*, 6, 24331. doi:10.1038/srep24331
- 619 Liu, F., Li, J. B., Wang, B., Liu, J., Li, T., Huang, G., & Wang Z. Y. (2018). Divergent El Niño
620 responses to volcanic eruptions at different latitudes over the past millennium. *Climate*
621 *Dynamics*, 50(9-10), 3799-3812. <https://doi.org/10.1007/s00382-017-3846-z>
- 622 Man, W., Zhou, T., & Jungclaus, J. H. (2014). Effects of large volcanic eruptions on global
623 summer climate and East Asian Monsoon changes during the last millennium: Analysis of MPI-
624 ESM simulations. *Journal of Climate*, 27(19), 7394-7409. doi:10.1175/jcli-d-13-00739.1
- 625 McKee, T. B., Doesken, N.J., & Kleist, J. (1993). *The relationship of drought frequency and*
626 *duration to time scale*. Paper presented at the Proceedings of the Eighth Conference on Applied
627 Climatology, American Meteorological Society, Anaheim, California.
- 628 PAGES 2k–PMIP3 group (2015). Continental-scale temperature variability in PMIP3
629 simulations and PAGES 2k regional temperature reconstructions over the past millennium.
630 *Climate of the Past*, 11(12), 1673-1699. doi:10.5194/cp-11-1673-2015
- 631 PAGES Hydro2k Consortium (2017). Comparing proxy and model estimates of hydroclimate
632 variability and change over the Common Era. *Climate of the Past*, 13(12), 1851-1900.
633 doi:10.5194/cp-13-1851-2017
- 634 Palmer, W. C. (1965). Meteorological Drought. *Weather Bureau*, 45, 1-58.
- 635 Robock, A. (2000). Volcanic eruptions and climate. *Reviews of Geophysics*, 38(2), 191-219.
- 636 Robock, A. (2015): Volcanoes: Role in climate. In North, G. R., Pyle, J., & Zhang, F. Q. (Eds),
637 *Encyclopedia of Atmospheric Sciences* (Vol. 2, pp. 105-111). San Diego, CA: Academic.
- 638 Schmidt, G. A., Jungclaus, J. H., Ammann, C. M., Bard, E., Braconnot, P., Crowley, T. J., et al.
639 (2011). Climate forcing reconstructions for use in PMIP simulations of the last millennium
640 (v1.0). *Geoscientific Model Development*, 4(1), 33-45. doi:10.5194/gmd-4-33-2011
- 641 Schmidt, G. A., Kelley, M., Nazarenko, L., Ruedy, R., Russell, G. L., Aleinov, I., et al. (2014).
642 Configuration and assessment of the GISS ModelE2 contributions to the CMIP5 archive. *Journal*
643 *of Advances in Modeling Earth Systems*, 6(1), 141-184. doi:10.1002/2013ms000265
- 644 Song, F., & Zhou, T. (2014). The climatology and interannual variability of East Asian Summer
645 Monsoon in CMIP5 coupled models: Does air–sea coupling improve the simulations? *Journal of*
646 *Climate*, 27(23), 8761-8777. doi:10.1175/jcli-d-14-00396.1
- 647 Stevenson, S., Fasullo, J. T., Otto-Bliesner, B. L., Tomas, R. A., & Gao, C. (2017). Role of
648 eruption season in reconciling model and proxy responses to tropical volcanism. *Proceedings of*

- 649 *the National Academy of Sciences of the United States of America*, 114(8), 1822-1826.
650 doi:10.1073/pnas.1612505114
- 651 Stevenson, S., Otto-Bliesner, B., Fasullo, J., & Brady, E. (2016). “El Niño Like” Hydroclimate
652 Responses to Last Millennium Volcanic Eruptions. *Journal of Climate*, 29(8), 2907-2921.
653 doi:10.1175/jcli-d-15-0239.1
- 654 Sun, W. Y., Liu, J., Wang, B., Chen, D. L., Liu, F., Wang, Z. Y., et al. (2018). A “La Niña-like”
655 state occurring in the second year after large tropical volcanic eruptions during the past
656 1500 years. *Climate Dynamics*, <https://doi.org/10.1007/s00382-018-4163-x>
- 657 Timmreck, C., Pohlmann, H., Illing, S., & Kadow, C. (2016). The impact of stratospheric
658 volcanic aerosol on decadal-scale climate predictions. *Geophysical Research Letters*, 43(2), 834-
659 842. doi:10.1002/2015gl067431
- 660 Trenberth, K. E., & Dai, A. (2007). Effects of Mount Pinatubo volcanic eruption on the
661 hydrological cycle as an analog of geoengineering. *Geophysical Research Letters*, 34(15),
662 L15702. doi:10.1029/2007gl030524
- 663 Wang, T., Guo, D., Gao, Y. Q., Wang, H. J., Zheng, F., Zhu, Y. L. et al. (2017). Modulation of
664 ENSO evolution by strong tropical volcanic eruptions. *Climate Dynamics*,
665 <https://doi.org/10.1007/s00382-017-4021-2>
- 666 Watanabe, M., Suzuki, T., O’ishi, R., Komuro, Y., Watanabe, S., Emori, S., et al. (2010).
667 Improved Climate Simulation by MIROC5: Mean States, Variability, and Climate Sensitivity.
668 *Journal of Climate*, 23(23), 6312-6335. doi:10.1175/2010jcli3679.1
- 669 Webb, R. W., Rosenzweig, C. E., & Levine, E. R. (2000). *Global soil texture and derived water-*
670 *holding capacities*. Data Set available from <http://www.daac.ornl.gov>. Oak Ridge National
671 Laboratory Distributed Active Archive Center. doi:10.3334/ORNLDAAAC/548
- 672 Wegmann, M., Brönnimann, S., Bhend, J., Franke, J., Folini, D., Wild, M., & Luterbacher, J.
673 (2014). Volcanic Influence on European Summer Precipitation through Monsoons: Possible
674 Cause for “Years without Summer”. *Journal of Climate*, 27(10), 3683-3691. doi:10.1175/jcli-d-
675 13-00524.1
- 676 Wu, D., Zhao, X., Liang, S., Zhou, T., Huang, K., Tang, B., & Zhao, W. (2015). Time-lag effects
677 of global vegetation responses to climate change. *Global Chang Biology*, 21(9), 3520-3531.
678 doi:10.1111/gcb.12945
- 679 Wu, T., Li, W., Ji, J., Xin, X., Li, L., Wang, Z., et al. (2013). Global carbon budgets simulated by
680 the Beijing Climate Center Climate System Model for the last century. *Journal of Geophysical*
681 *Research: Atmospheres*, 118(10), 4326-4347. doi:10.1002/jgrd.50320
- 682 Zambri, B., & Robock, A. (2016). Winter warming and summer monsoon reduction after
683 volcanic eruptions in Coupled Model Intercomparison Project 5 (CMIP5) simulation.
684 *Geophysical Research Letters*, 43, 10920-10928. doi:10.1002/2016GL070460

- 685 Zambri, B., Robock, A. N. L. A., & Slawinska, J. (2017). Northern Hemisphere winter warming
686 and summer monsoon reduction after volcanic eruptions over the last millennium. *Journal of*
687 *Geophysical Research-Atmospheres*, 122, 7971-7989. doi:10.1002/2017JD026728
- 688 Zhang, D., Blender, R., & Fraedrich, K. (2012). Volcanoes and ENSO in millennium
689 simulations: global impacts and regional reconstructions in East Asia. *Theoretical and Applied*
690 *Climatology*, 111(3-4), 437-454. doi:10.1007/s00704-012-0670-6
- 691 Zhou, T., Wu, B., Wen, X., Li, L., & Wang, B. (2008). A fast version of LASG/IAP climate
692 system model and its 1000-year control integration. *Advances in Atmospheric Sciences*, 25(4),
693 655-672. doi:10.1007/s00376-008-0655-7
- 694 Zhuo, Z., Gao, C., & Pan, Y. (2014). Proxy evidence for China's monsoon precipitation response
695 to volcanic aerosols over the past seven centuries. *Journal of Geophysical Research:*
696 *Atmospheres*, 119(11), 6638-6652. doi:10.1002/2013JD021061

Figure 1.

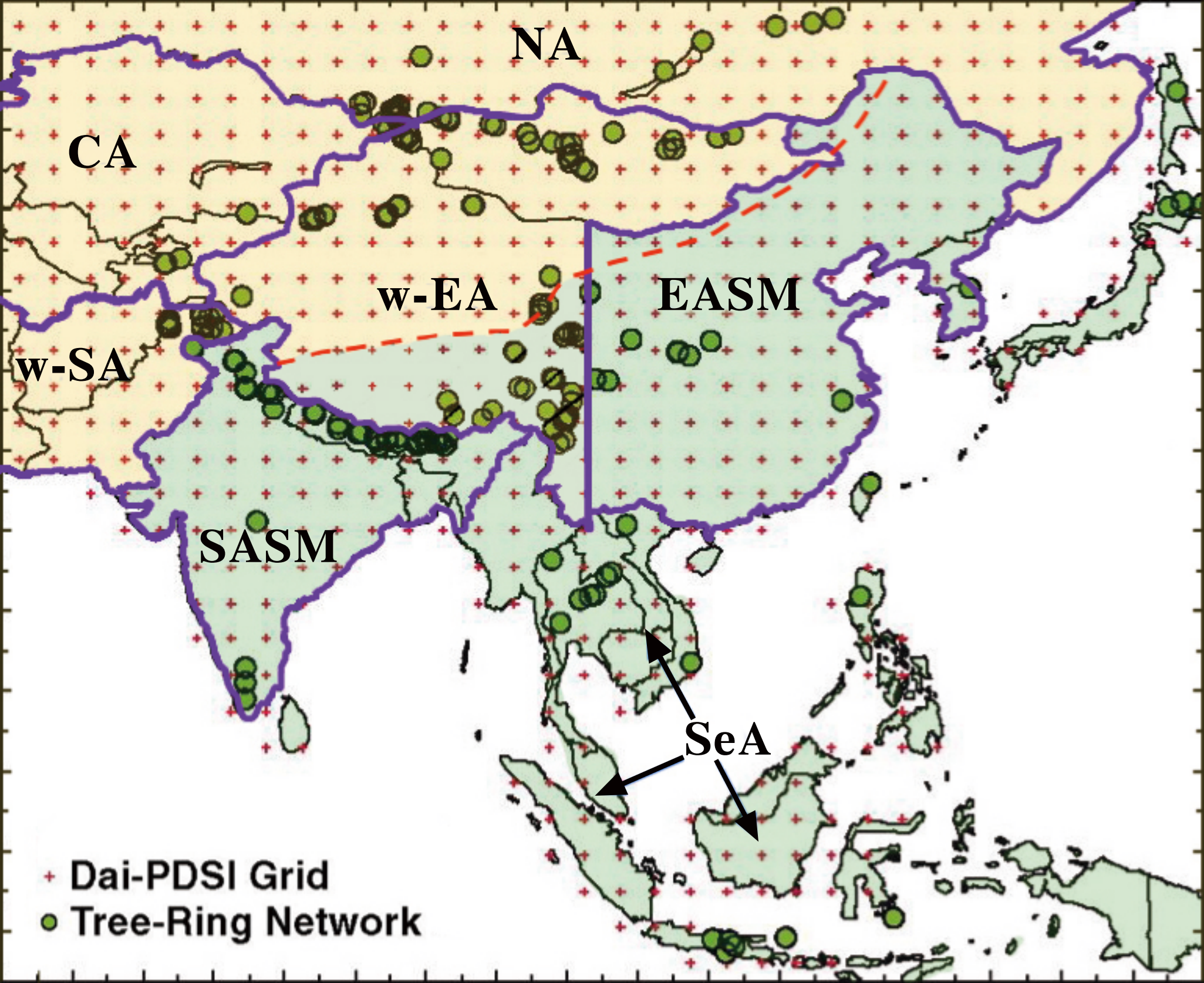


Figure 2.

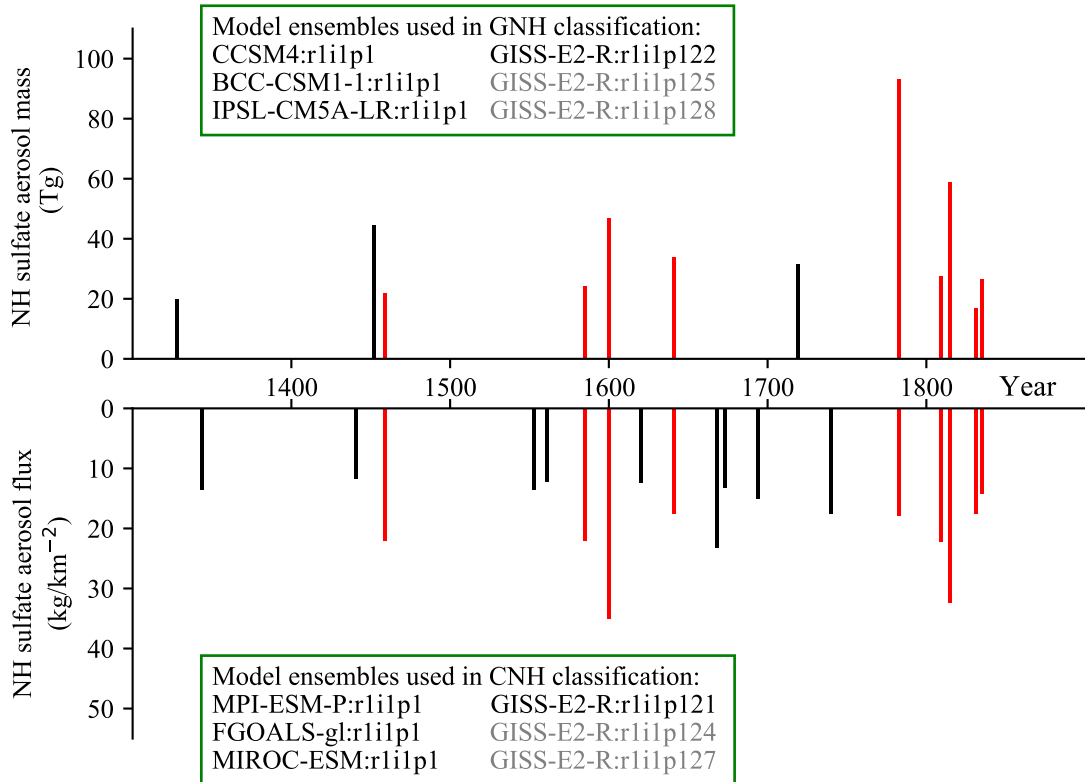
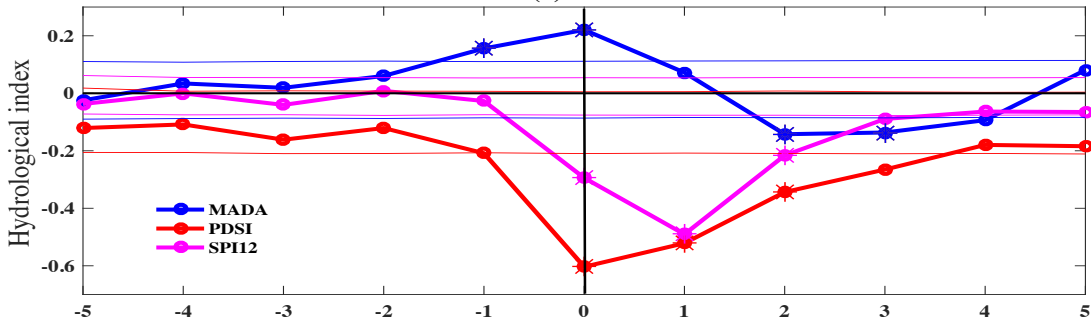


Figure 3.

(a) GNH



(b) CNH

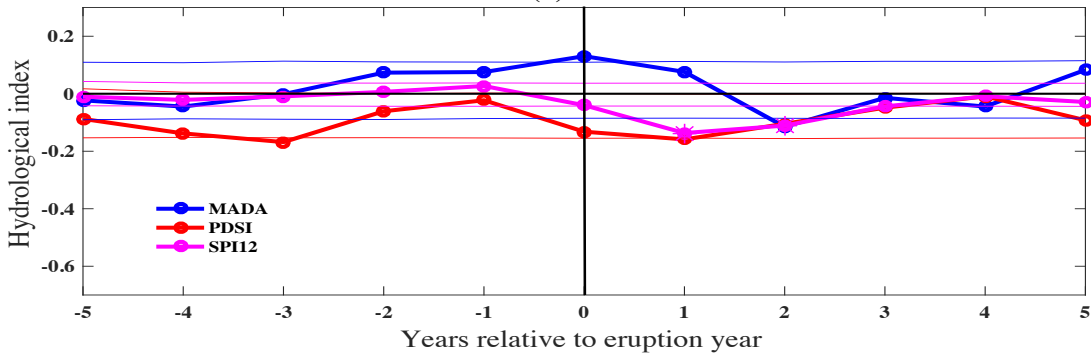


Figure 4.

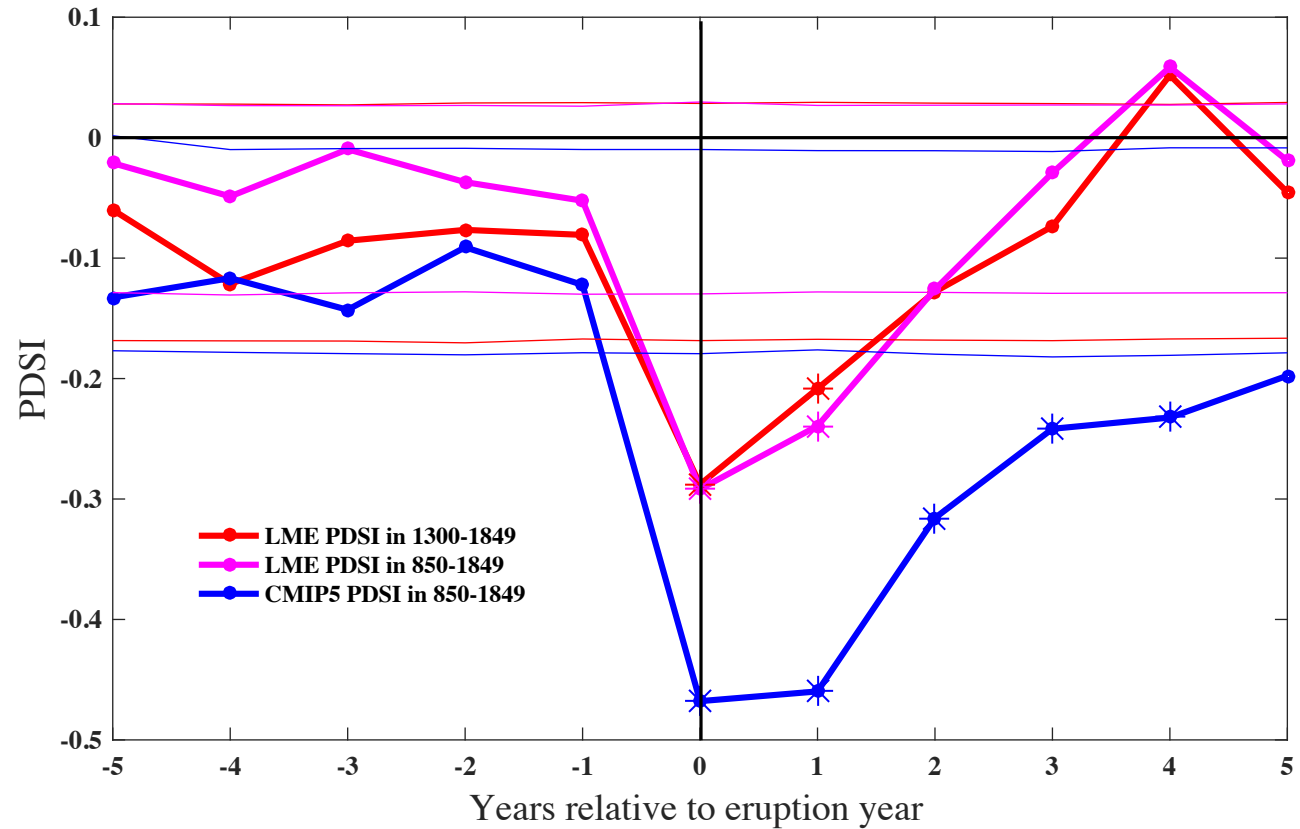
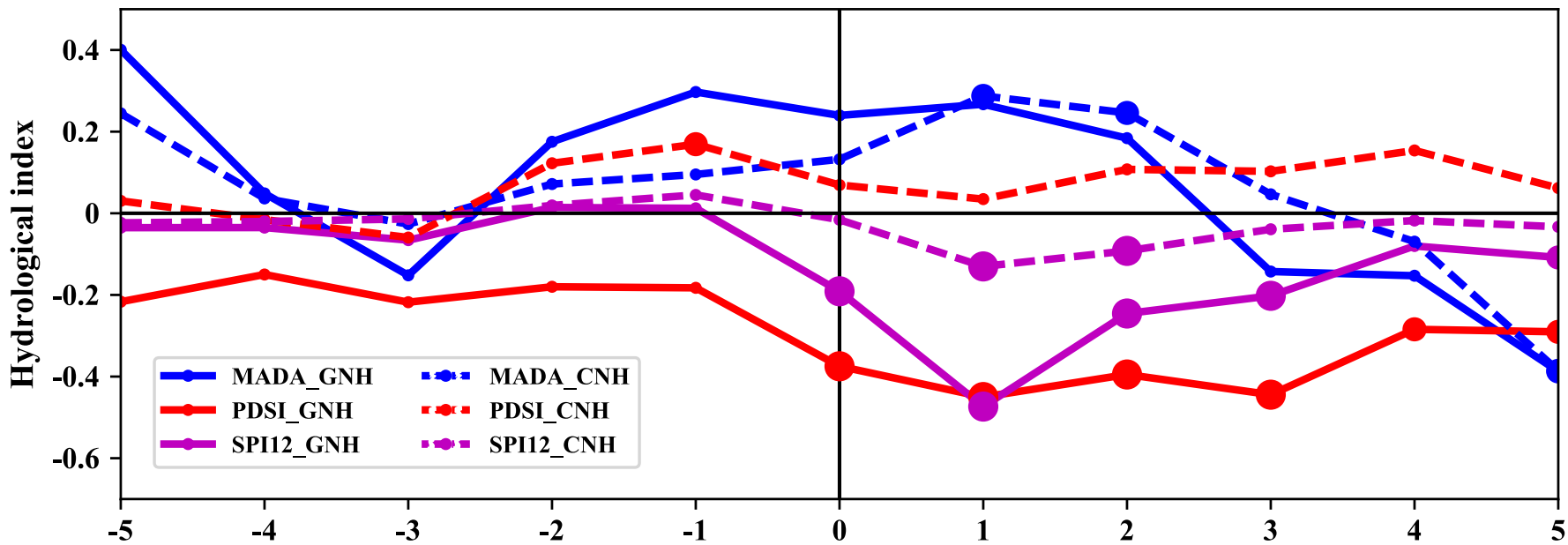


Figure 5.

(a) Westerlies-dominated subregion



(b) Monsoon-dominated subregion

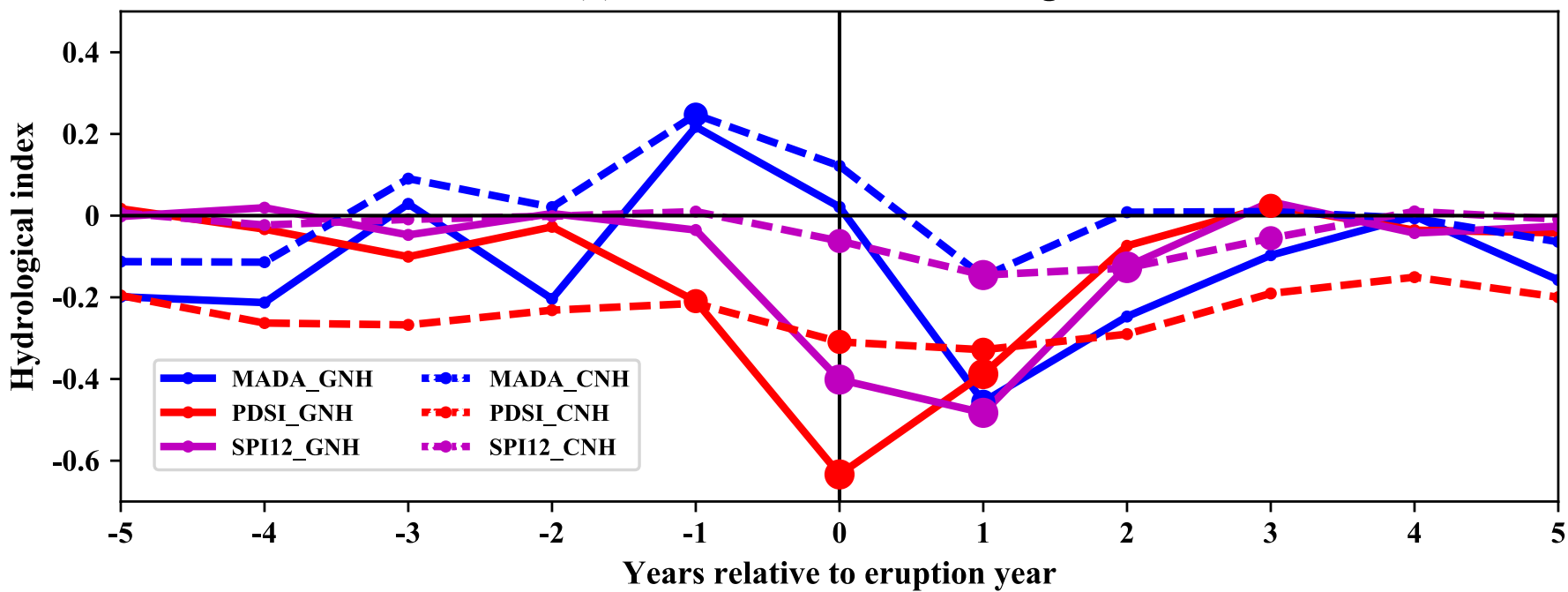
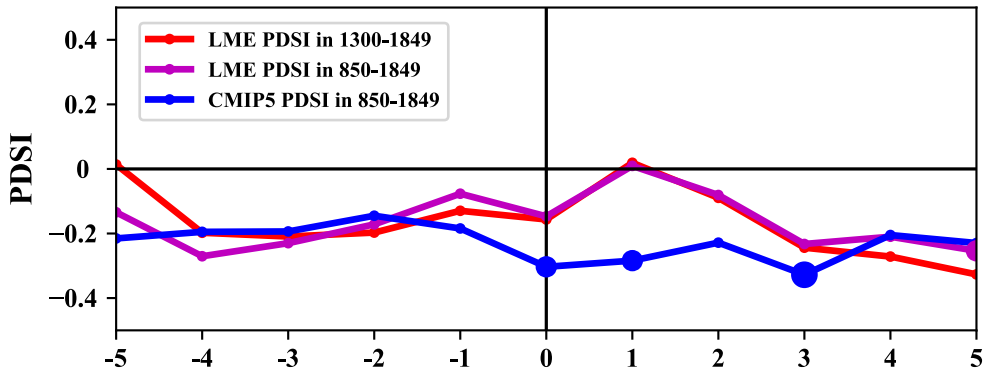


Figure 6.

(a) Westerlies-dominated subregion



(b) Monsoon-dominated subregion

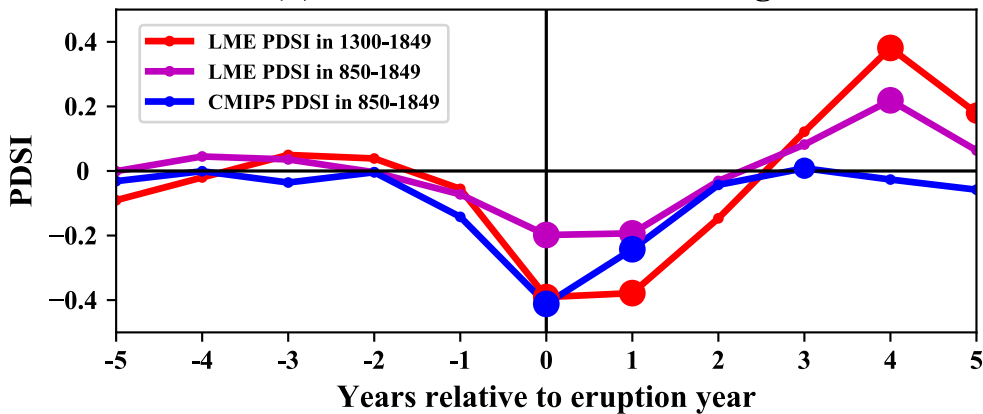
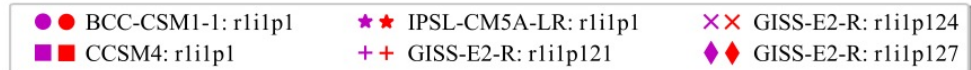
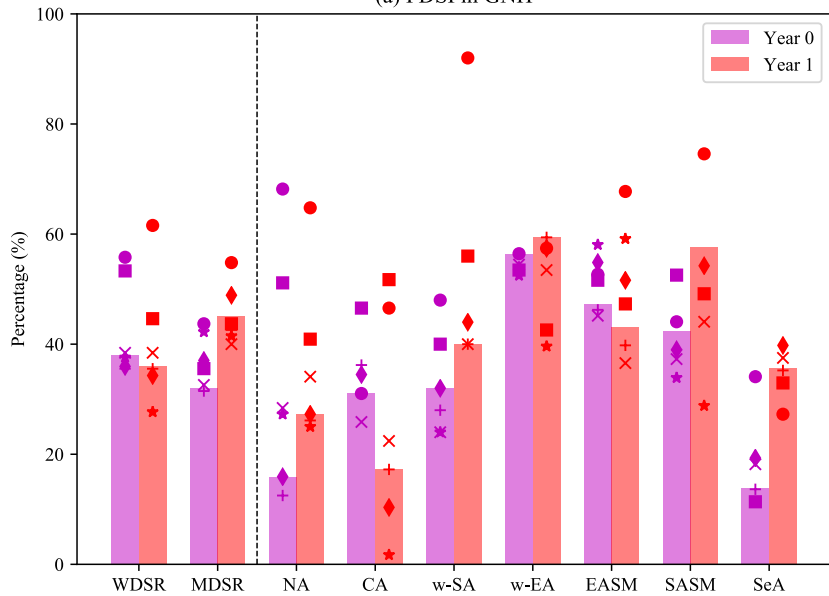
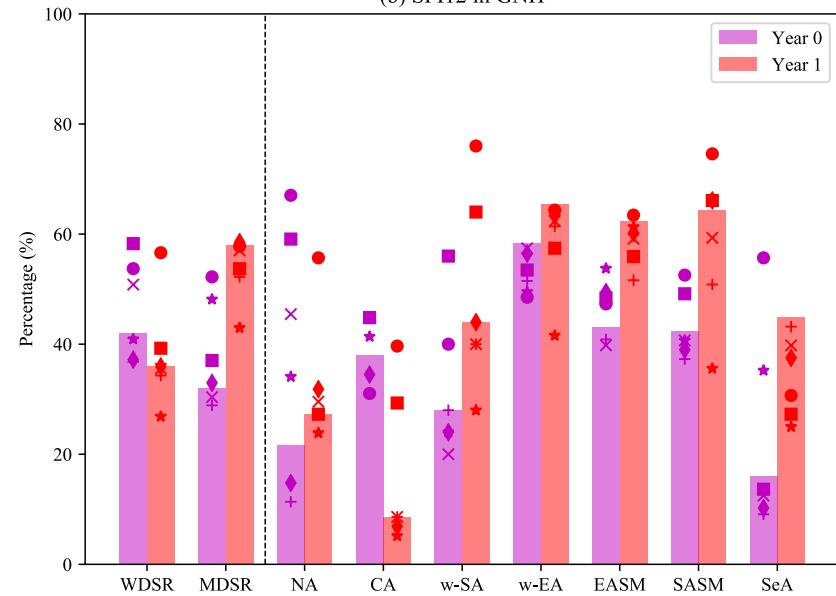


Figure 7.

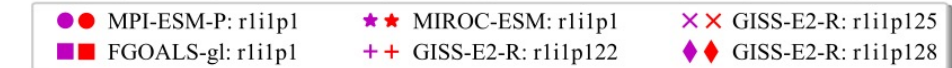
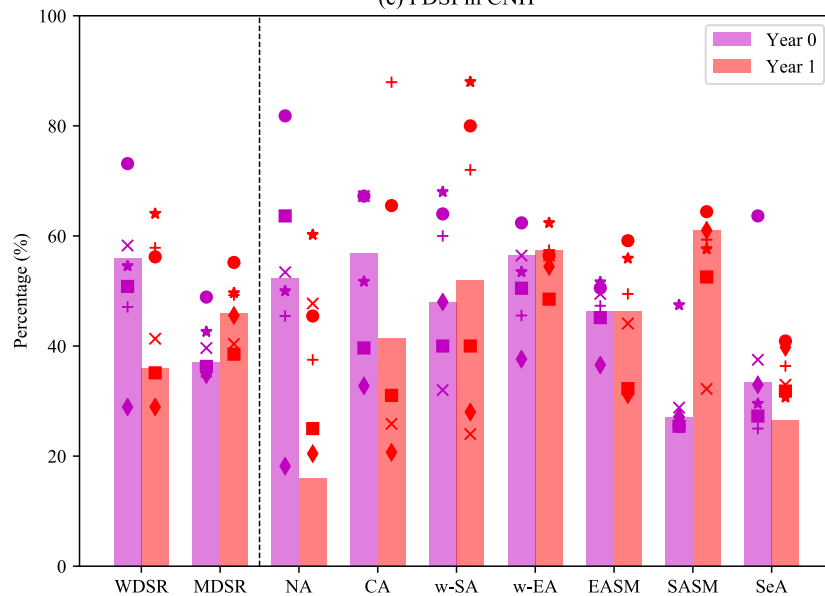
(a) PDSI in GNH



(b) SPI12 in GNH



(c) PDSI in CNH



(d) SPI12 in CNH

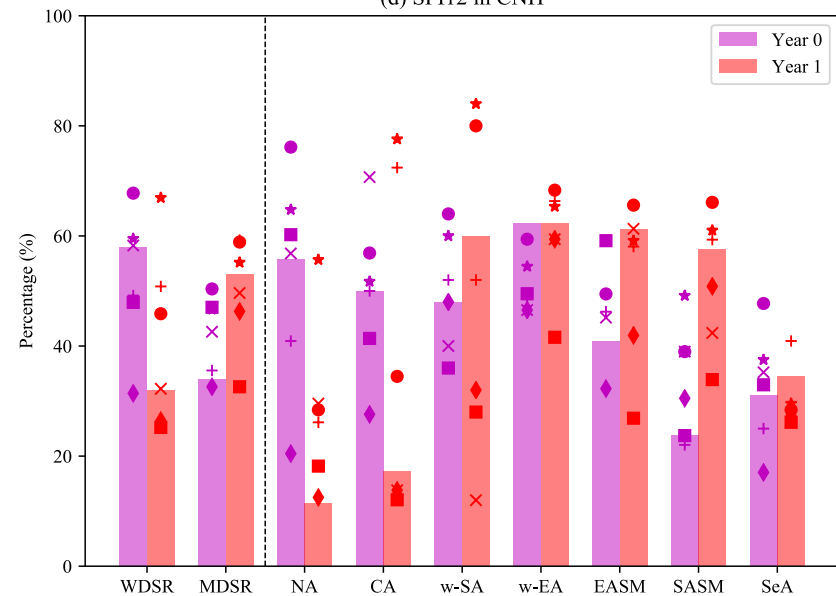


Figure 8.

(a) MADA PDSI

(b) CMIP5 PDSI

(c) CMIP5 SPI12

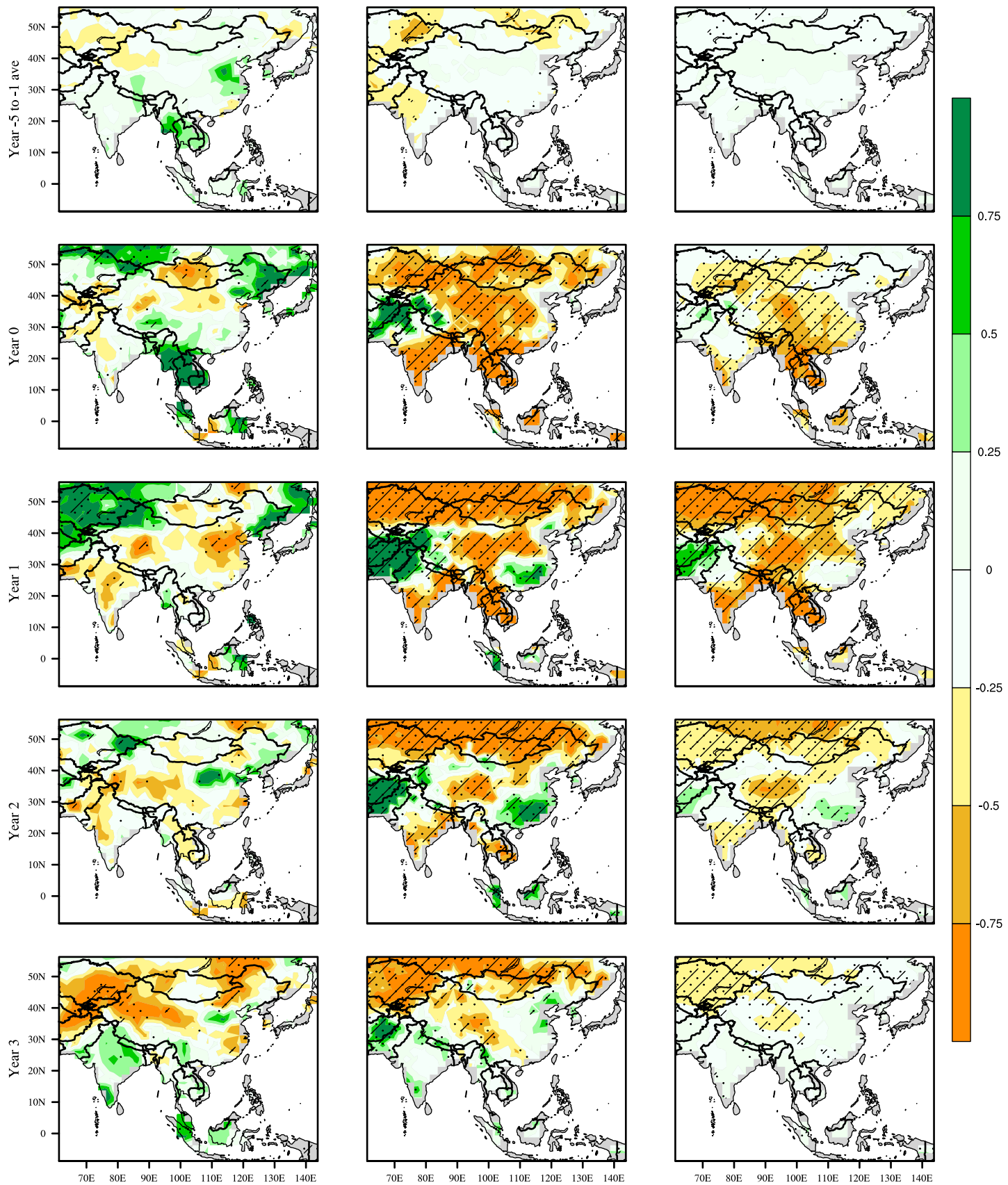


Figure 9.

(a) MADA PDSI

(b) CMIP5 PDSI

(c) CMIP5 SPI12

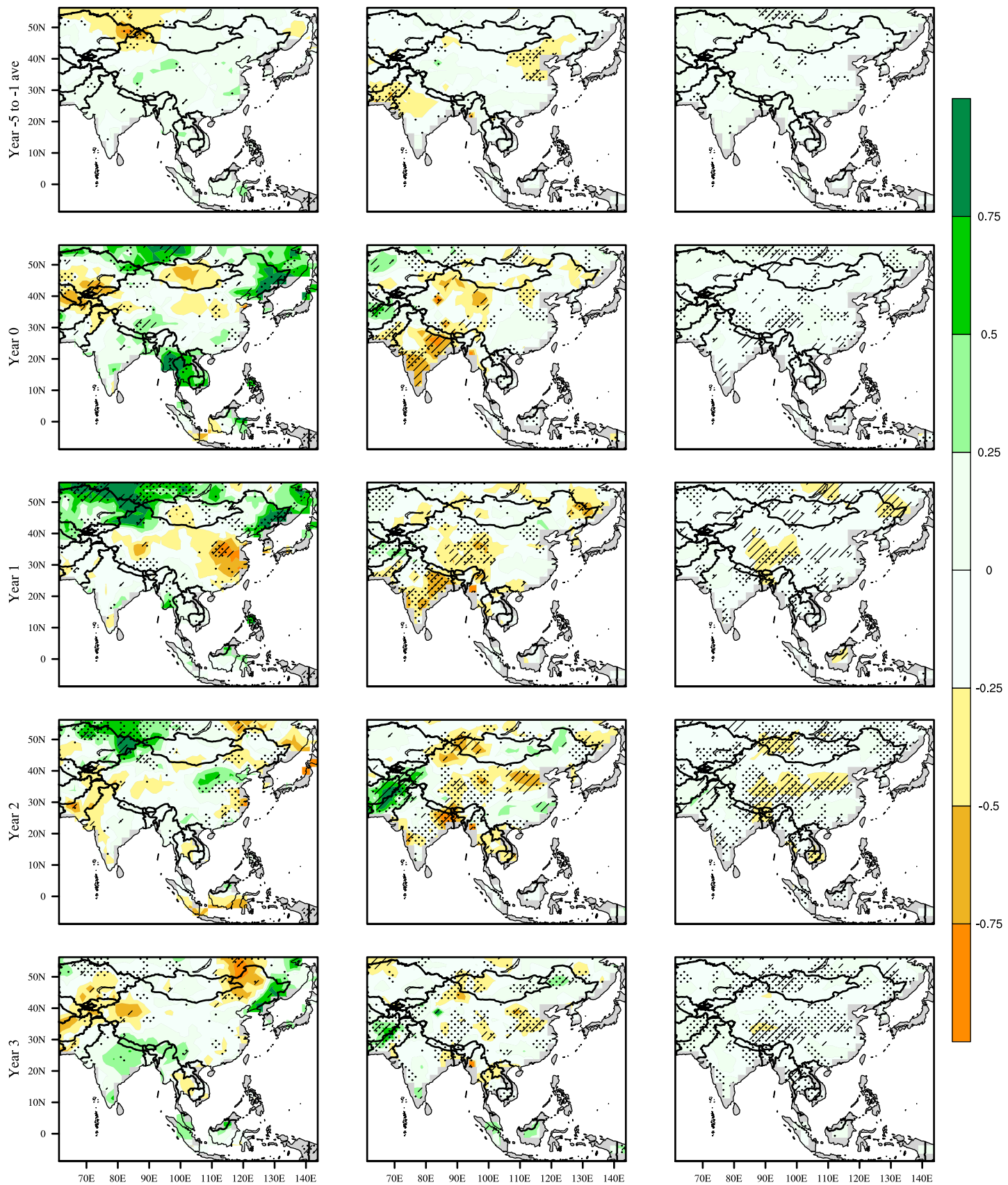


Figure 10.

(a) LME PDSI in 1300-1849

(b) LME PDSI in 850-1849

(c) CMIP5 PDSI in 850-1849

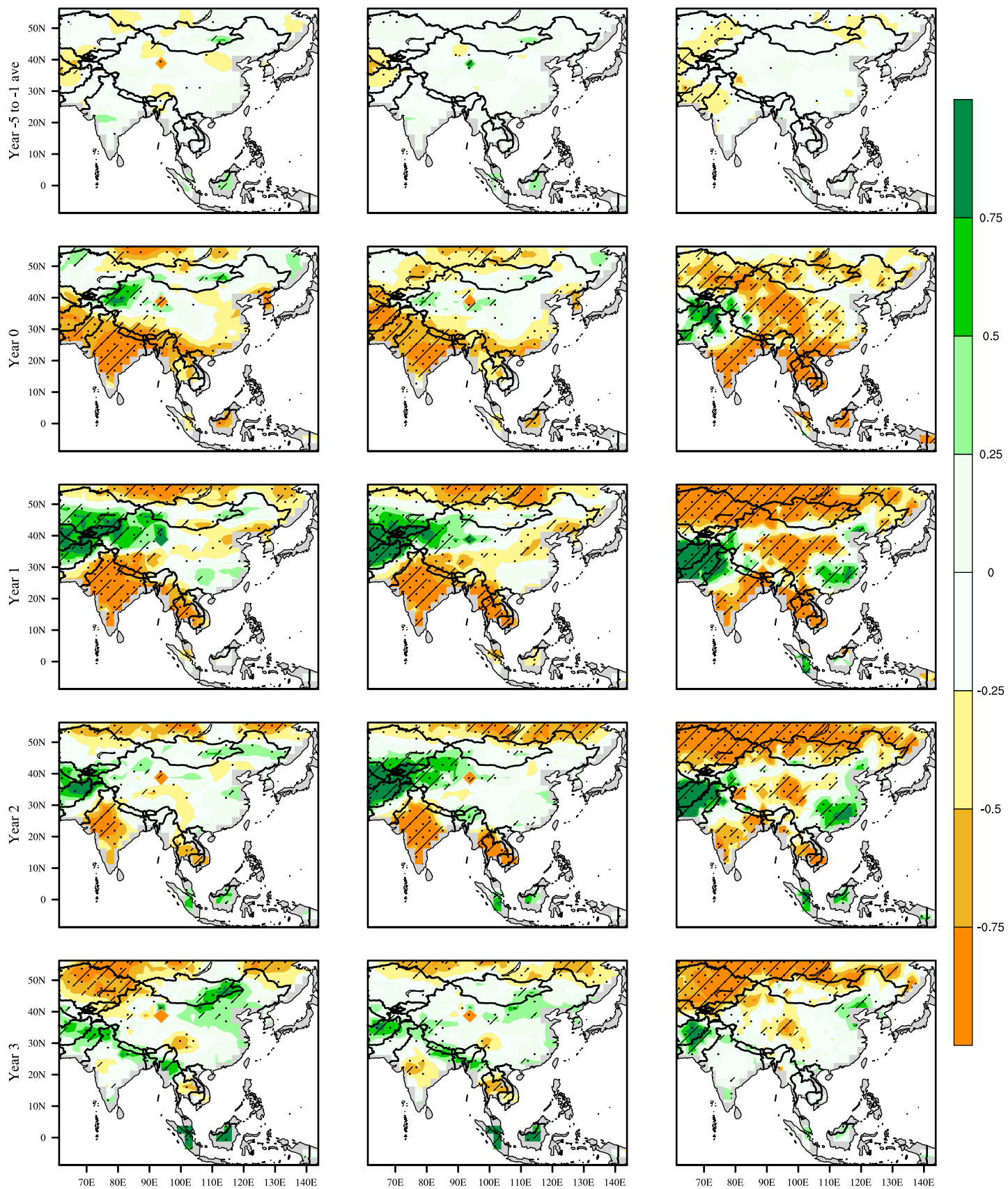


Figure 11.

